Critical Conditions for Jumping Droplets

Quoc Vo and Tuan Tran*
School of Mechanical & Aerospace Engineering, Nanyang Technological University, 50 Nanyang Avenue, 639798, Singapore

(Received 14 January 2019; published 10 July 2019)

A droplet initially overstretched on a solid substrate pulls back to lower the contact area and may jump away from the substrate. The condition to realize such macroscopic behaviors is often dictated by microscopic characteristics, such as contact-line pinning, in nontrivial ways. Here we theoretically and experimentally reveal the hidden contribution of contact-line pinning in forming the critical condition for detachment of a droplet from a solid substrate, among other dominating hydrodynamical effects. Our results demonstrate the relation between classical theories on contact-line pinning and various droplet manipulating applications in microfluidics and bioprinting.

DOI: 10.1103/PhysRevLett.123.024502

The ability to generate motion of a sessile droplet initially resting on a solid substrate directly ties to the dynamics of the three-phase contact line (CL) between the liquid interface and the substrate, among other factors such as viscous dissipation in the bulk liquid and capillarity. The motion of a moving CL is resisted by viscous dissipation and pinning of part of the CL to the surface. While CL dissipation shares similar viscosity and velocity dependences with the dissipation in the bulk flow [1–5], CL pinning originates from physical or chemical heterogeneity of the surface. In other words, CL pinning has little to do with the bulk liquid properties but depends more strongly on microscopic characteristics of the surface. Theoretical models considering the relation between CL pinning and surface heterogeneity typically describe CL motion as a series of hopping events over defects characterized by an energy barrier E_b and a typical size γ [6]. Subsequently, experimental studies focusing on the relation between CL pinning and microscopic characteristics of the defects start to emerge [7]. Although it is now possible to incorporate microscopic models of CL pinning into understanding of wetting phenomena such as contact angle hysteresis, a phenomenon in which the apparent receding and advancing contact angles differ from that at equilibrium [8], many macroscopic wetting phenomena remain elusive due to entangled contributions from both CL pinning and bulk flows [9]. A prominent example is the role of CL pinning in detachment conditions of droplets from solid substrates.

In this Letter, we study how CL pinning contributes to the critical conditions for sessile droplets to detach from a substrate. We induce the detachment of droplets using the electrowetting effect. A droplet initially resting on a substrate with a contact angle θ_0 spreads to a new equilibrium state with a smaller contact angle $\theta_e < \theta_0$ when a voltage difference V is applied between the droplet and the substrate [10]. With a sufficient surface energy difference between the initial equilibrium state and the new one, turning off V causes the droplet to retract towards the initial equilibrium state and detach from the substrate.

In our experiment, the substrate is an indium tin oxide (ITO) coated glass electrode covered with an amorphous polymers layer (Teflon AF 1600, DuPont) of thickness

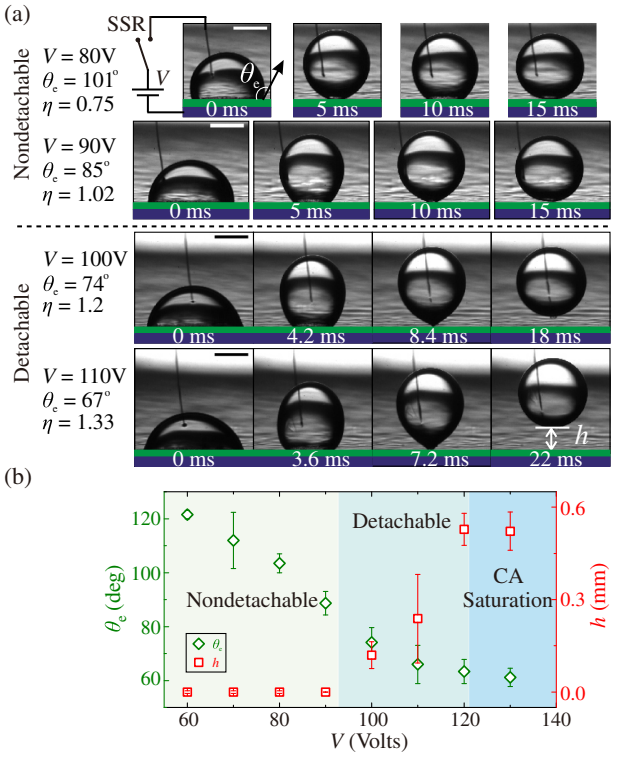

FIG. 1. (a) Snapshots showing droplets retracting without jumping (top two panels), and droplets retracting and subsequently jumping from the substrate (bottom two panels). The scale bars represent 0.5 mm. (b) Plot showing the dependence of θ_e (diamonds, left axis) and the corresponding jumping height h (squares, right axis) on the applied voltage V. The viscosity of droplets is $\mu = 1.0$ mPa s.

$d = 2.2$ μm and dielectric constant $\epsilon = 1.93$. To induce the electrowetting effect for a droplet on the substrate, a 18 μm diameter tungsten wire is dipped into the bulk of the droplet. The wire and the electrode are connected to a power supply through a solid-state relay (SSR) to close the circuit. The liquid used to generate droplets is an aqueous glycerin solution consisting of glycerol, DI water, and 0.125 M sodium chloride having viscosity varied from 1.0 mPa s to 68.7 mPa s [11]. The droplet radius R is varied from 0.25 mm to 1.25 mm. We immerse droplets and the electrode in a pool of silicone oil with viscosity $\mu_o = 1.8$ mPa s. The temperature of the pool is kept fixed at 20 ± 0.5 °C to maintain consistent experimental conditions.

In Fig. 1(a), we show several representative snapshots of actuated droplets after the applied voltage V is turned off. The actuation is recorded by a camera (SAX2, Photron) typically running at 5000 frames per second. We observe that there is a threshold value of V for detachment to occur, e.g., a droplet of radius 0.5 mm detaches from the substrate when $V > 90$ V [Fig. 1(a)]. We note that without contact angle (CA) saturation, θ_e directly relates to V following the Young-Lippmann equation: $\cos\theta_e - \cos\theta_0 = \epsilon\epsilon_0 V^2 (2\sigma d)^{-1} = \eta$ [10], where ϵ_0 is the permitivity of free space, σ the interfacial tension between the droplet's liquid and the outer oil, and $\theta_0 = 160° \pm 2.5°$. By changing V from 50 V to 110 V, we vary the so-called electrowetting number η from 0.26 to 1.46 [11]; the range of η varies slightly between liquids of different viscosities due to the dependence of σ on glycerol concentration [11]. To ensure that electrowetting actuation is free of CA saturation, we set the upper limit of V slightly below the saturation voltage V_s [Fig. 1(b)]; V_s varies from 100 to 120 V depending on the working liquid [11].

Whether an actuated droplet detaches from the substrate depends on the interplay between the parameters R, μ, and η. In Fig. 2, we show the transition between the two regimes, detachable and nondetachable. On the one hand, for a fixed viscosity, e.g., $\mu = 1.0$ mPa s, the required value of η for detachment reduces with increasing R [Fig. 2(a)], implying that smaller droplets require higher excessive surface energy to detach. On the other hand, for a fixed droplets radius, e.g., $R = 0.5$ mm, η at the transition increases with μ and is limited at $\mu = 8.2$ mPa s [Fig. 2(b)]. As a result, within our explored parameter range, it is not possible to induce detachment for $\mu \geq 8.2$ mPa s.

To examine the transition between the two regimes, we consider energy conversion between two actuating stages: the initial stage, defined shortly after V is released but before any hydrodynamical response [Fig. 1(a), $t = 0$], and the final stage, set after the droplet is completely detached from the substrate. Assuming sphericality of the droplet at the final stage, the difference in surface energy between the two stages is $\Delta E_s = \sigma(A_1 - A_2) + \pi r_e^2(\sigma_{sl} - \sigma_{so})$, where A_1 and A_2, respectively, are the droplet surface

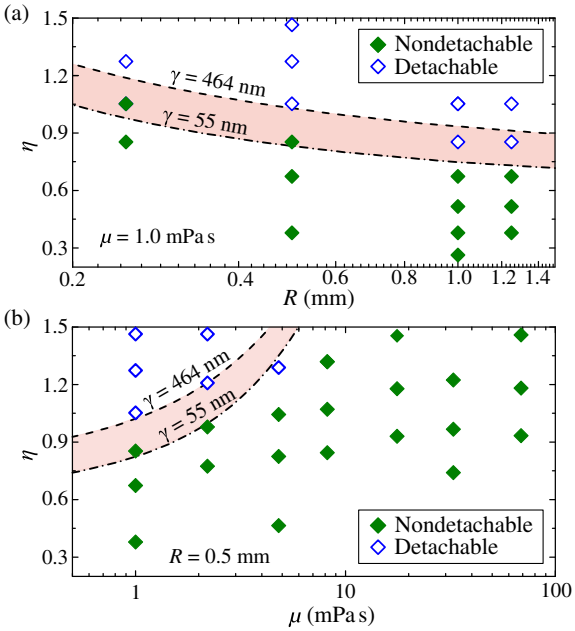

FIG. 2. Phase diagrams showing the detachable (open diamonds) and nondetachable regimes (solid diamonds) for droplets of (a) fixed viscosity ($\mu = 1.0$ mPa s), and (b) fixed radius ($R = 0.5$ mm). The dashed-dotted line and dashed line are predictions of the transition to the detachable regime using Eq. (5) with $\gamma = 55$ nm and $\gamma = 464$ nm, respectively.

areas at the initial and final stages, and r_e is the contact radius at the initial stage. Here σ_{so} and σ_{sl} are interfacial tensions of the solid-oil and solid-liquid interfaces, respectively. Using the Young's relation $\sigma_{so} - \sigma_{sl} = \sigma\cos\theta_0$ and noting that $A_1 - A_2$ can be expressed as a function of θ_e and r_e [12], we obtain

$$\Delta E_s = \left(\frac{2}{1+\cos\theta_e} - \frac{4}{\beta^2} - \cos\theta_0\right)\sigma\pi r_e^2 = \alpha\sigma\pi r_e^2. \quad (1)$$

Here, since $\beta = r_e R^{-1}$ is a function of θ_e [4], α is also a function of θ_e, which directly relates to η following the Young-Lippmann equation. If we denote E_v as the viscous dissipation during actuation and E_{cl} as the stored energy by CL elasticity [13], the excess surface energy ΔE_s has to overcome the sum of E_v and E_{cl} to enable detachment. We note that the change in energy of the electrical double layer is negligible [11,14]. In other words, at the transition between the detachable and nondetachable regimes, the following condition holds:

$$\Delta E_s = E_v + E_{cl}. \quad (2)$$

To determine the viscous dissipation E_v, we separately estimate contributions from the region near the substrate, the bulk liquid, and the vicinity of the CL. We note that the boundary layer near the substrate has a characteristic thickness $\zeta \approx 0.665(\nu r_{ct} u_{ct}^{-1})^{1/2}$, where ν is the kinematic

viscosity, and u_{ct} and r_{ct} are the CL velocity and CL radius, respectively. The measured retraction rate $u_{ct}r_{ct}^{-1}$ is $\approx 207 \pm 12\ s^{-1}$ for liquids with $\mu \leq 17.6$ mPa s [15] and $u_{ct}r_{ct}^{-1} \sim \mu^{-1/2}$ for liquids with $\mu \geq 17.6$ mPa s [11]. In addition, the flows outside of the boundary layer ($z > \zeta$) can be approximated as potential flows, consistent with measurements using particle imaging velocimetry (PIV) of the flow inside a droplet of $R = 0.5$ mm and $\mu = 4.8$ mPa s [Fig. 3(a)] [11,16], as well as reported numerical simulations [5]. The velocity fields obtained using PIV enable us to determine the dissipation rate $\dot{T}_s$ caused by shear stress near the surface ($z \leq \zeta$) and the dissipation rate $\dot{T}_b$ for the bulk flow ($z > \zeta$) [11]. The rate of CL dissipation by friction is estimated as $\dot{T}_c \sim 2\pi\lambda r_{ct}u_{ct}^2$, where r_{ct} and u_{ct} are measured experimentally and $\lambda = C(\mu\mu_o)^{1/2} = 96.7$ mPa s is the CL friction coefficient [2,17]. The constant $C = 32.9 \pm 3.2$, specific to the tested substrate, was reported previously [4].

In Fig. 3(b), we show a comparison between the dissipation rates for a representative case in which $R = 0.5$ mm, $\mu = 4.8$ mPa s, $\eta = 1.28$, and the estimated boundary layer thickness is $\zeta = 96$ μm. We observe that $\dot{T}_c$ dominates over both $\dot{T}_b$ and $\dot{T}_s$ for the duration $t < 6$ ms, which spans the first half of the retraction phase where the CL velocity is high. Here, $\dot{T}_b$ and $\dot{T}_s$ are calculated from PIV measurement [11]. Integrating individual dissipation rates over the entire actuation time gives $T_b \approx 2.65 \times 10^{-9}$ N m, $T_s \approx 4.24 \times 10^{-9}$ N m, and $T_c \approx 18.40 \times 10^{-9}$ N m. Since the total viscous dissipation $E_v = T_b + T_s + T_c$, the contribution from CL dissipation is 72.7% of E_v, indicating that dissipation at the CL overwhelms those in the bulk and the boundary layer.

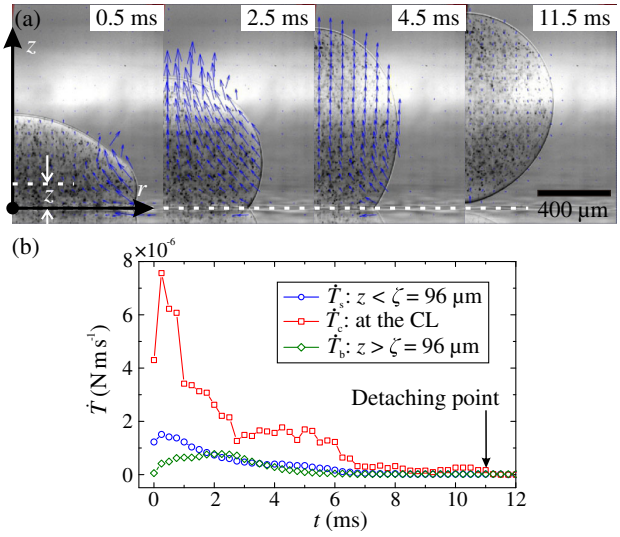

FIG. 3. (a) Snapshots showing the velocity field of a droplet having $R = 0.5$ mm, $\mu = 4.8$ mPa s, and $\eta = 1.28$ after the voltage is released. (b) Plot showing the dissipation rates at the boundary layer $\dot{T}_s(t)$, at the CL $\dot{T}_c(t)$, and in the bulk $\dot{T}_b(t)$.

Similar calculations for various actuation conditions confirm the dominating role of CL dissipation and are consistent with previous studies on transient wetting dynamics [2,5]. As a result, we attribute CL dissipation as the main contributing factor to the total viscous dissipation and obtain $E_v \approx \int \dot{T}_c dt \sim \pi\lambda r_e^2 U$, where U is the characteristic CL velocity [18].

There are two major dynamical regimes with distinct characteristic CL velocities U: the overdamped and the underdamped regimes [4]. In the former one, viscous forces dominate, resulting in a characteristic timescale $\tau_o = r_e U^{-1} \sim \lambda r_e \eta^{-1}\sigma^{-1}$. The CL velocity therefore is estimated as $U \sim \eta\sigma\lambda^{-1}$. This leads to the expression $E_v \sim \eta\sigma\pi r_e^2$ of the total viscous dissipation at the CL. Substituting this expression of E_v and that of ΔE_s [Eq. (1)] into Eq. (2) reveals that the jumping condition only satisfies if either $\alpha = \eta$ (i.e., $\theta_e = 0$) and $E_{cl} = 0$, or $E_{cl} < 0$. Both of these conditions are not realistically possible [11]. Thus, we infer that in the overdamped regime, the CL friction dissipates all the stored surface energy ΔE_s, preventing droplet detachment.

In the underdamped regime, the characteristic timescale is $\tau_u = \pi\rho^{1/2}R^{3/2}(\eta\sigma)^{-1/2}$, where ρ is the density of the working liquid [4]. This results in the characteristic velocity $U \sim r_e\tau_u^{-1}$. The total viscous dissipation at the CL, therefore, can be estimated as

$$E_v \sim \lambda \frac{r_e}{\tau_u}\pi r_e^2 = \eta\sigma\frac{\tau_o}{\tau_u}\pi r_e^2 = \eta\xi\sigma\pi r_e^2. \tag{3}$$

Here $\xi = \tau_o\tau_u^{-1}$ is the damping ratio used to differentiate two dynamical behaviors: $\xi > 1$ in the overdamped regime and $\xi < 1$ in the underdamped regime [4]. As it is only possible for the surface energy difference $\Delta E_s = \alpha\sigma\pi r_e^2$ to be larger than the CL dissipation $E_v \sim \eta\xi\sigma\pi r_e^2$ for $\xi < 1$ [19], droplet detachment only occurs in the underdamped regime. In other words, the underdamped dynamics provides a necessary condition for droplet detachment.

To obtain the sufficient condition for droplet detachment, we now discuss the term E_{cl}, which represents energy accumulation due to pinning and subsequent stretching of the liquid interface at CL vicinity. The mechanism to induce and store elastic energy works as follows: as the CL recedes, the liquid interface is stretched at pinning sites, i.e., microscopic heterogeneities on the surface. The pinning of the CL and the resulting surface stretching at such pinning sites can be modeled as an elastic force per unit length along the CL [13,20]: $f \sim \pi\sin^2\theta_r\sigma\ln^{-1}L\gamma^{-1}$, where θ_r is the receding contact angle [21], L is the macroscopic cutoff length of the CL region and is usually approximated using the droplet radius R, and γ is the defect size depending on the substrate's morphology and chemical homogeneity [13]. For common smooth surfaces, the value of γ varies from molecular size to few micrometers [13], causing $\ln L\gamma^{-1}$ to vary from 15 to 4 if the macroscopic

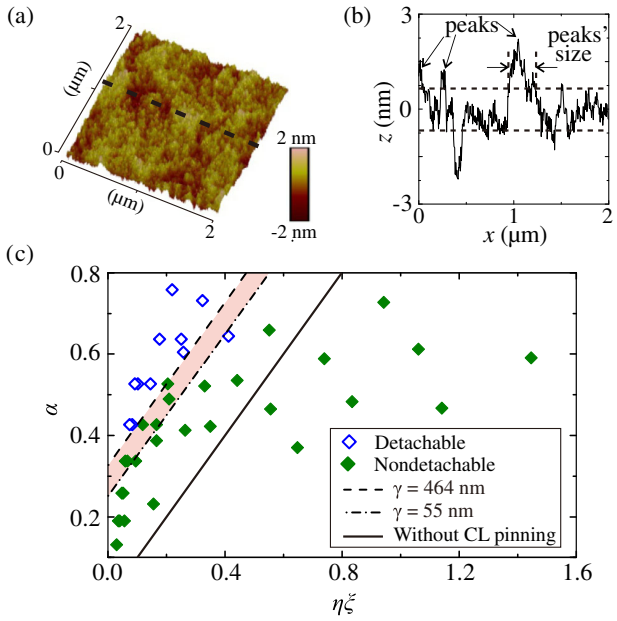

FIG. 4. (a) A representative image obtained using AFM showing the surface morphology of a Teflon-coated substrate. (b) Plot showing the elevation z along the dashed line in (a). (c) Phase diagram of detachable (open diamonds) and nondetachable (solid diamonds) regimes plotted using the variables $\eta\xi$ and α. The shaded area shows the transitional extent caused by variation in γ.

cutoff length L takes the value of droplet radius [3], e.g., $L = R \sim 0.5$ mm in our case. To estimate the value of γ, we use atomic force microscopy (AFM) to examine the substrates used in our experiment [Fig. 4(a)]. For a sample size of $5\ \mu\text{m} \times 5\ \mu\text{m}$, the maximum peak height is $\approx$5.74 nm, and the surface roughness is $\approx$0.6 nm, similar to the reported characteristics of Teflon coated surfaces [22]. Any surface feature protruding beyond standard deviation limits [horizontal dashed lines, Fig. 4(b)], is classified as a "peak." The topological defect size γ is then approximated using the peaks's lateral size, which varies from 55 nm to 464 nm [11]. The defect density is estimated from the peak density, which is $\approx 9.2 \pm 0.6$ peaks per μm^2. Equivalently, the interspacing between defects is $\delta \approx 500$ nm.

The relation between the defect interspacing δ and the characteristic deformation ϕ of a pinned CL determines whether the induced elastic energy is dissipated or accumulated. Here ϕ, defined as the maximum deformation possibly caused by a defect site, can be estimated as $\phi \sim (L\gamma)^{1/2}$ [13]. Choosing $L = R \approx 0.5$ mm and $\gamma \approx 100$ nm gives $\phi \sim 7\ \mu$m, much larger than the estimated value of δ ($\delta \approx 500$ nm). A direct consequence of the relation $\phi > \delta$ is that the moving CL, after depinned from a defect, is not totally relaxed by the time it reaches the next defect; the CL therefore is further and further stretched as it moves past defects. In other words, the elastic energy generated due to pinning and depinning of the CL is not dissipated but accumulated in the liquid interface [11,23]. This is consistent with the observation that a droplet always deforms significantly (and takes the shape of an inverted teardrop) right before detachment. As a result, the total stored energy E_{cl} is estimated by integrating f over the CL's sweeping area πr_{e}^2:

$$E_{\text{cl}} \sim f\pi r_{\text{e}}^2 \sim \frac{\pi \sin^2\theta_{\text{r}}}{\ln L\gamma^{-1}} \sigma \pi r_{\text{e}}^2. \tag{4}$$

Eventually, the surface energy difference ΔE_{s} has to overcome both the viscous dissipation E_{v} and the accumulated elastic energy E_{cl} for the droplet to detach from the substrate. By substituting Eqs. (1), (3), and (4) into Eq. (2), we obtain the condition at the transition to the detachable regime:

$$\alpha = \eta\xi + \frac{\pi \sin^2\theta_{\text{r}}}{\ln L\gamma^{-1}}. \tag{5}$$

This condition reflects the contributions from the excess surface energy (represented by α), the CL dissipation ($\eta\xi$), and the CL pinning ($\pi \sin^2\theta_{\text{r}} \ln^{-1} L\gamma^{-1}$) in enabling detachment. We note that ξ weakly depends on η [4] and therefore can be considered independent of η. In Fig. 4(c), we show a plot of the transitions predicted by Eq. (5) using $\theta_{\text{r}} \approx 121.7°$ [21], and limiting values of γ, i.e., $\gamma = 55$ nm (dashed-dotted line) and $\gamma = 464$ nm (dashed line). The predicted transitions are in remarkable agreement with the experimental data obtained in the two regimes. In particular, although the shaded area bounded by the limiting values of γ implies the uncertainty of defect size estimation, it is consistent with scattered data from both the detachable and nondetachable regimes. We note that *if* CL pinning is not taken into account, i.e., Eq. (5) becomes $\alpha = \eta\xi$, then the theory vastly underestimates the excess surface energy required for detachment [Fig. 4(c), solid line]. This comparison strongly attests the critical role of CL pinning in predicting the transition to detachment. In the special case that $\xi = 0$, i.e., the working liquids are inviscid, the detachment condition [Eq. (5)] depends only on the initial contact angle θ_{e} and surface heterogeneity reflected through γ.

In conclusion, to a good approximation the main factors resisting an overstretched droplet to detach from a solid surface are localized at the moving contact line. These include a dissipative effect, i.e., CL friction, and an elastic effect, i.e., elastic energy accumulated at liquid interface due to CL pinning. Balancing the sum of these resistive effects with the excess surface energy initially imposed on the system, e.g., by the electrowetting effect, gives rise to the critical condition for droplet detachment. Regardless of how initial excess surface energy is induced, e.g., by coalescence [24] or by impacting inertia, our analysis of the attendant effects in CL dynamics has a strong bearing in

diverse applications such as liquid repellant [25] thermal diode [26], and dropwise condensation heat transfer [27].

This study is supported by Nanyang Technological University and the Agency for Science, Technology and Research (A*STAR) under its Pharos Funding Scheme (Grant No. 1523700102).

*Corresponding author.
ttran@ntu.edu.sg

[1] Q. Vo and T. Tran, Phys. Rev. E **97**, 063101 (2018).
[2] A. Carlson, G. Bellani, and G. Amberg, Europhys. Lett. **97**, 44004 (2012).
[3] S. Moulinet, C. Guthmann, and E. Rolley, Eur. Phys. J. B **37**, 127 (2004).
[4] Q. Vo, H. Su, and T. Tran, Sci. Rep. **8**, 836 (2018).
[5] A. Carlson, M. Do-Quang, and G. Amberg, J. Fluid Mech. **682**, 213 (2011).
[6] T. D. Blake and J. M. Haynes, J. Colloid Interface Sci. **30**, 421 (1969).
[7] W. Zhang, N. Li, K. Bohinc, P. Tong, and W. Chen, Phys. Rev. Lett. **111**, 168304 (2013); X. Ma, W. Chen, Z. Wang, Y. Peng, Y. Han, and P. Tong, Phys. Rev. Lett. **110**, 078302 (2013); Y. J. Wang, S. Guo, H. Y. Chen, and P. Tong, Phys. Rev. E **93**, 052802 (2016); D. Guan, Y. J. Wang, E. Charlaix, and P. Tong, Phys. Rev. Lett. **116**, 066102 (2016).
[8] A. Giacomello, L. Schimmele, and S. Dietrich, Proc. Natl. Acad. Sci. U.S.A. **113**, E262 (2016).
[9] A. Cavalli, D. J. Preston, E. Tio, D. W. Martin, N. Miljkovic, E. N. Wang, F. Blanchette, and J. W. M. Bush, Phys. Fluids **28**, 022101 (2016).
[10] F. Mugele and J.-C. Baret, J. Phys. Condens. Matter **17**, R705 (2005).
[11] See Supplemental Material at http://link.aps.org/supplemental/10.1103/PhysRevLett.123.024502, specifically Section I for more information on properties of materials and saturation voltages, Section II for more data and calculation of the electrowetting number η, Section III for the estimation of the electrical double layer energy, Section IV for additional experimental results and analysis of the retraction rate, Section V for additional experimental results of using PIV, Section VI for more experimental results and analysis of the receding contact angles, Section VII for more experimental results and analysis of the AFM measurement, Section VIII for analysis of the elastic energy of the CL, and Fig. 5 for the calculation of α and η for a full range of the contact angle θ_e.
[12] The dependence of $A_1 - A_2$ on θ_e and r_e can be fully expanded as $A_1 - A_2 = 2(1+\cos\theta_e)^{-1}\pi r_e^2 - 4\pi R^2$.
[13] J. F. Joanny and P. G. D. Gennes, J. Chem. Phys. **81**, 552 (1984); P. G. De Gennes, Rev. Mod. Phys. **57**, 827 (1985).
[14] D. G. Hall, J. Colloid Interface Sci. **108**, 411 (1985); J. K. Moon, J. Jeong, D. Lee, and H. K. Pak, Nat. Commun. **4**, 1487 (2013); D. C. Grahame, Chem. Rev. **41**, 441 (1947).
[15] D. Bartolo, C. Josserand, and D. Bonn, J. Fluid Mech. **545**, 329 (2005).
[16] W. Thielicke and E. J. Stamhuis, J. Open Source Software **2**, e30 (2014).
[17] To calculate the friction coefficient λ for a representative case in which $\mu = 4.8$ mPa s, we use $\lambda = C(\mu\mu_o)^{1/2}$, an empirical relation that was validated for μ in the range from 8.2 mPa s to 615.0 mPa s [1]; Z. Wang, D. van den Ende, A. Pit, R. Lagraauw, D. Wijnperlé, and F. Mugele, Soft Matter **13**, 4856 (2017); A. Carlson, G. Bellani, and G. Amberg, Phys. Rev. E **85**, 045302(R) (2012).
[18] The CL dissipation can be calculated as $\int \dot{T}_c dt = -2\pi\lambda \int u_{ct} r_{ct} dr_{ct}$. Here $u_{ct} = -dr_{ct}/dt$ is the retracting velocity and is estimated using the characteristic CL velocity U. Integrating the CL dissipation from r_e to 0 results in $\int \dot{T}_c dt \sim 2\pi\lambda U \int_0^{r_e} r_{ct} dr_{ct} = \pi r_e^2 \lambda U$.
[19] Since $\xi < 1$ for the underdamped behavior, it is possible that $\alpha - \eta\xi > 0$, or $\Delta E_s > E_v$. In order words, detachment is possible in the underdamped regime.
[20] T. Ondarçuhu and M. Veyssié, Nature (London) **352**, 418 (1991); M. Delmas, M. Monthioux, and T. Ondarçuhu, Phys. Rev. Lett. **106**, 136102 (2011).
[21] During the retracting stage, θ_r increases from θ_e and quickly reaches a plateau ($\approx$130°), independent of θ_e. Thus, we use $\theta_r \approx 121.7 \pm 13.4°$.
[22] J. G. Petrov, J. Ralston, M. Schneemilch, and R. A. Hayes, Langmuir **19**, 2795 (2003); E. Rolley and C. Guthmann, Phys. Rev. Lett. **98**, 166105 (2007); C. J. Drummond, G. Georgaklis, and D. Y. C. Chan, Langmuir **12**, 2617 (1996).
[23] J. H. Snoeijer, B. Andreotti, G. Delon, and M. Fermigier, J. Fluid Mech. **579**, 63 (2007); G. Delon, M. Fermigier, J. H. Snoeijer, and B. Andreotti, J. Fluid Mech. **604**, 55 (2008).
[24] H. Vahabi, W. Wang, J. M. Mabry, and A. K. Kota, Sci. Adv. **4**, eaau3488 (2018).
[25] K. M. Wisdom, J. A. Watson, X. Qu, F. Liu, G. S. Watson, and C.-H. Chen, Proc. Natl. Acad. Sci. U.S.A. **110**, 7992 (2013).
[26] J. B. Boreyko, Y. Zhao, and C.-H. Chen, Appl. Phys. Lett. **99**, 234105 (2011).
[27] N. Miljkovic, R. Enright, Y. Nam, K. Lopez, N. Dou, J. Sack, and E. N. Wang, Nano Lett. **13**, 179 (2013).